*Kuwait J. Sci. & Eng.* **25**, 1998

# A distributed circuit model for back contacted silicon solar cells

MOUSTAFA Y. GHANNAM, EMMANUEL VAN KERSCHAVER* AND JOHAN F. NIJS*

*Electrical and Computer Engineering Dept, Kuwait University, P.O. Box 5969, 13060 Safat, Kuwait*

* *Interuniversity MicroElectronics Center, IMEC, Kapeldreef 75, 3001 Leuven, Belgium*

## ABSTRACT

The performance of solar cells with dual $n^+$ emitter and p base contacts at the back side fabricated on industrial (cost effective) silicon solar cell material is investigated by means of circuit modelling. The model is based on dividing the structure into sections which are modelled as distributed circuit segments each consisting of a diode, a current source and appropriate segment series resistances. The parameters of the circuit elements are determined from one dimensional simulations using the device simulator PC-1D. The circuit analysis is carried out analytically and confirmed by computer simulations using the circuit simulator HSPICE. The effects of the cell thickness, surface recombination velocity and diffusion length are investigated. Finally, the back side $n^+/p$ area aspect ratio that optimally resolves the trade-off between maximum $n^+$ area and minimum series resistance is determined. It is shown that the efficiency of back emitter cells with a standard thickness is 1.5% smaller than that of front emitter cells. On the other hand, the back emitter cell appears to be a serious contender for silicon cells thinner than 50 $\mu$m. The analysis demonstrates that the back emitter cell should have good bulk quality and good surface passivation. It is also shown that the optimum separation between the n and p back metal contact is as large as 1.5–1.8 mm. Moreover, it is shown that the best performance is obtained with minimum back emitter contact width, and with two extra emitter contact stripes added parallel to the central emitter contact.

## I. INTRODUCTION

Moving all the metal contacts in solar cells to the back side eliminates the front grid obscuration losses, reduces the series resistance, simplifies and allows the automation of the module assembly process by removing the front to back cell stringing, and leads to a higher cell packing density. In such a case, however, the emitter is moved to the back side. The idea of dual n and p back contact solar cells with interdigitated metal contact lines is relatively old (Lammert & Schwartz 1977, Schwartz 1982) and has been implemented more recently in back n and p point contact cells (Sinton *et al.* 1985, Sinton & Swanson 1987) operating under highly concentrated sunlight fabricated on high quality substrates using advanced technology

and resulted in a conversion efficiency of 28% (Sinton *et al.* 1985) which is the highest efficiency ever achieved by a silicon solar cell. Recently, the emitter wrap-through cell has been presented as a potentially serious candidate for back contact cells to be implemented in cost effective silicon solar cell processes (Gee *et al.* 1993, 1994).

In the present work, the performance of back emitter silicon solar cells fabricated on industrial silicon material following a cost effective process is investigated. Only operation under one-sun, global AM1.5 illumination spectrum, which is used as a standard for terrestrial solar cell testing, is considered. A one dimensional study is carried out using the PC-1D device simulator (Basore & Clugston 1996) in order to compare the performance of the front emitter cells with that of the back emitter cells. From such a study reasonable conditions are extracted for proper back emitter cell operation. A circuit model is then used to investigate the performance of the back emitter cell taking into consideration the two dimensional aspect of the dual back contact configuration. An analytical solution of the proposed circuit is elaborated and the results are confirmed numerically using the computer circuit simulator HSPICE.

## II. BACK EMITTER SOLAR CELL STRUCTURE

### II.1. Description

The cross sections of the back emitter solar cell structure under study are sketched in Fig. 1 (a and b), while Fig. 1 (c) displays the cross section of the standard front emitter cell investigated in the present study for the purpose of comparison. Due to symmetry only a unit cell representing half of the structure is investigated. The $n^+$ emitter and the p base contacts are interdigitated. In Fig. 1 (a), the back side emitter surface is fully metallized, while in Fig. 1 (b) the back emitter contact occupies a minimum area and the rest of the emitter surface is passivated with a silicon dioxide layer. The major concern here is to optimize the emitter width for a minimum base contact width. Since we deal here with a cost effective process, namely screen-printing technology, the minimum line width is approximately 60 μm. Therefore, the

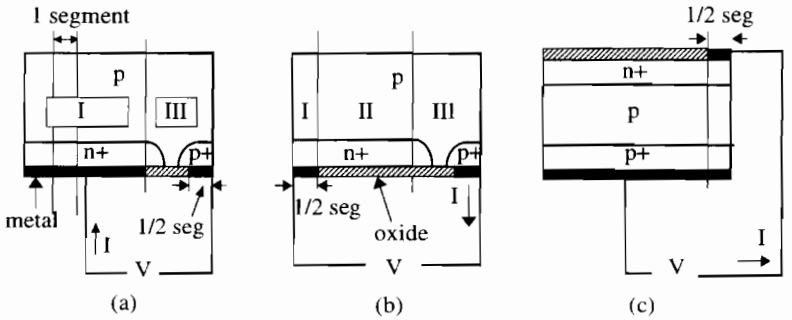


**Fig. 1.** (a) and (b) represent back emitter unit cells with the emitter divided into section I (metallized emitter surface) and section II (oxide-passivated emitter surface). Section III includes half a segment (30 μm) corresponding to the metal base contact region, as well as the separation between the base contact opening and the emitter opening on the mask or screen. In (a) the whole emitter opening surface is metallized, in (b) the emitter contact width is minimum (1/2 segment). Sketch (c) represents a front emitter unit cell with a minimum emitter contact width (1/2 segment width).

base contact width is fixed at this value. Also the spacing between the edge of the p-base contact and the $n^+$ emitter diffusion window on the screen is assumed to be 60 μm.

The p-type base has a uniform resistivity of 1 Ω.cm which is the most common resistivity used in industrial silicon solar cell processes. Three major parameters control the performance of back emitter cells: (1) the minority carrier diffusion length in the base, (2) the cell thickness, and (3) the recombination velocity at the p-type front surface. Two values of the diffusion length $L_n$ are investigated in the present analysis corresponding to silicon material used in the cost effective process: $L_n = 200$ μm as a maximum value for polycrystalline (multicrystalline) silicon, and $L_n = 300$ μm as a maximum value for Cz monocrystalline. The cell thickness is treated as an independent variable for which an optimum value should be found. Relatively low values of $S_{n,\,eff}$ must be ensured for proper operation of back emitter cells. Since the front p-type surface has the same relatively low doping as the bulk region, good oxide passivation should offer low values of $S_{n,\,eff}$ (Eades & Swanson 1985). Furthermore, it has been proven that p-type surface recombination can be significantly reduced by implementing a high/low $p^+/p$ junction as in the Front Surface Field cell (Von Roos & Anspaugh 1978) or a floating $n^+/p$ junction as in the Tandem Junction cell (Chiang *et al.* 1978, Ghannam 1991). In the present analysis two indicative values $S_{n,\,eff} = 100$ cm/s and 1000 cm/s are investigated.

The back emitter sheet resistance is chosen to be 35 Ω/square which is low enough to avoid high lateral series resistance. Although such a value is too low for standard front emitter solar cells, it can be reasonable for back emitter cells since the emitter has a negligible influence on the photogenerated current. In addition, the dark current of back emitter cells is dominated by injection into the base and hence the effect of the surface recombination velocity at the $n^+$ emitter surface is negligible. The value of $S_p$ at the oxidized emitter surface is assumed to be 1000 cm/s.

Finally, all the incident light is coupled into the back side emitter cell except the loss of light by reflection from the front surface. A uniform average reflection loss of 4% is assumed for the back emitter cell.

## II.2. One dimensional analysis: comparison between back emitter and front emitter cells

Comparison between the one dimensional performance of the back emitter and front emitter cells is carried out by means of numerical calculations using the PC-1D device simulator (Basore & Clugston 1996). For the comparison to be valid, the back emitter cell and the front emitter cell are assumed to be fabricated on an identical material and under similar processing conditions. The front emitter sheet resistance is equal to 80 Ω/square which is typical for a high efficiency industrial selective (composite) emitter cell (Szlufcik *et al.* 1991, Ghannam *et al.* 1997). The recombination velocity at the $n^+$ emitter surface, $S_p$, as well as the effective recombination velocity at the p-type base surface, $S_{n\,eff}$, are assumed to be equal in both front and back emitter cells. The value of the former is fixed at 1000 cm/s, while two values are considered for $S_{n,\,eff}$ : 100 and 1000 cm/s. Finally, unlike the back emitter cell in which only 4% of the light was not coupled into the cell due to reflection from its front surface, an extra 8% of the light is not coupled into the front emitter cell due to the shading caused by the front metal contact pattern.

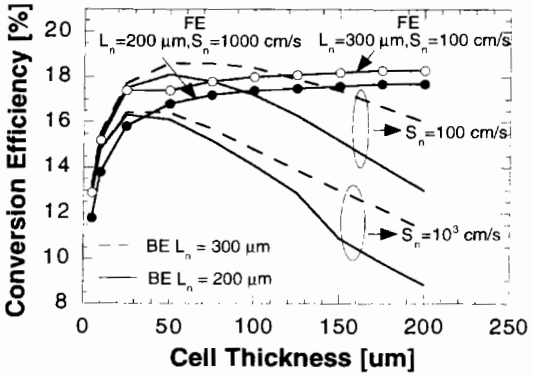


**Fig. 2.** Conversion efficiency calculated one dimensionally using PC-1D as a function of the cell thickness for back emitter (BE) and front emitter (FE) cell.

The resulting conversion efficiency for both types of cells is plotted in Fig. 2 as a function of the cell thickness. As opposed to the front emitter cell, the conversion efficiency of the back emitter cell shows a peak at a certain optimum thickness. Such optimum thickness is small and not practical when the front surface recombination velocity $S_{n,\,eff}$ is large. Even when $S_{n,\,eff} = 1000$ cm/s, which is usually considered not to be excessively large, the efficiency of the back emitter cell can never reach that of a normal thickness front emitter cell. On the other hand, low values of $S_{n,\,eff}$ leads to a maximum back emitter cell efficiency comparable to or even exceeding the highest efficiency reached by a front emitter cell. For instance, when $S_{n,\,eff} = 100$ cm/s and with a diffusion length $L_n$ of 300 µm, the highest efficiency reached by the front emitter cell is 18.3% for thicknesses larger than 150 µm while the maximum efficiency of the back emitter cell under the same conditions is 18.6% in the thickness range 50 to 80 µm. The optimum back emitter cell thickness is even below this range and its performance degrades with respect to that of a front emitter cell as the diffusion length decreases. This result shows that the potential of back emitter silicon solar cells is great in thin wafer solar cells and in thin silicon film solar cells. Such a result has an important significance since the tendency in the silicon solar cell industry today is towards these types of thin cells due to the continuously growing market and diminishing volume of available silicon feedstock. Even for present technology, the results shown here indicate that an efficiency of 17.9% is calculated for a 125 µm thick back emitter cell which is slightly less than the 18.3% maximum efficiency achieved by the front emitter cell. Note that the efficiency of a 125 µm thick front emitter cell is also 17.9%. It is worth mentioning that for a more usual thickness of 180 µm, the results of the one dimensional calculations displayed in Fig. 2 indicate that the efficiency of an optimized back emitter cell is 1.5% in absolute value smaller than that of the maximum front emitter cell efficiency.

## III. EQUIVALENT CIRCUIT MODEL OF THE BACK EMITTER CELL

### III.1. Description

The conversion efficiency of the back emitter cell calculated in the previous section using a one dimensional analysis is optimistic because it does not take into con-

sideration losses caused by the lateral current flow between the n and p contacts situated on the same side. More accurate calculations for such a structure should be carried out using two-dimensional device simulations. Such simulations require very long computational time especially when light generation is included. In the present section an approximate approach in which combined one dimensional calculations and circuit modelling substitute two dimensional calculations is proposed.

The structure to be modelled is represented by the unit cell sketched in Fig. 1(b) and is assumed to extend 1 cm normal to the page. The unit cell is divided vertically into three adjacent distinct sections representing: (I) a solar cell with a back side metal contacted $n^+$ emitter surface, (II) a solar cell with a back side oxide passivated $n^+$ emitter surface, and (III) a solar cell with a back side emitter (the lateral edge of unit cell emitter) and a back side base contact. Since the lateral extension of these sections, especially section I and section II, can be relatively wide, further division of these sections into identical narrow segments is necessary. The width of each segment is chosen to be 60 μm wide which is based on the minimum screenprinting line width. Section III is described by at least one segment 90 μm wide consisting of the metal p-type contact with a minimum line width of 30 μm (1/2 segment due to symmetry), and one standard 60 μm wide segment for the minimum separation between the p base contact and the emitter diffusion opening on the screen. The total area of the unit cell can be changed by varying the number of segments of section I and/or of section II. Note that section I represents the n contact region and hence must be represented with at least a 30 μm wide segment (due to symmetry). On the other hand, section II can be totally omitted in case the emitter surface is fully metallized as in Fig. 1 (a). The number of segments can be freely varied taking the above mentioned constraints into consideration.

As shown in Fig. 3, each segment is now modelled by a classical solar cell equivalent circuit consisting of a current source, a diode and two series resistances $R_{s,p}$ and $R_{s,n}$ representing the resistance of the lateral current path in the base region and in the $n^+$ emitter region, respectively. The unit cell containing the three different sections can now be represented by the circuit sketched in Fig. 4. Note that it is assumed that the fully metallized emitter surface in section I provides a uniform current density. Also, in the equivalent circuit of the same section, $R_{s,n}$ is omitted because all the n-type nodes of the corresponding segments are short circuited by the metal contact.

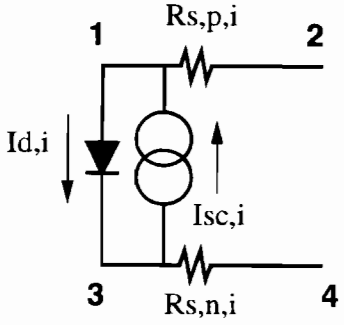


**Fig. 3.** Equivalent circuit model for one general basic segment No. i of the back emitter unit cell structure sketched in Fig. 1 (a and b) showing the convention for the node numbers.

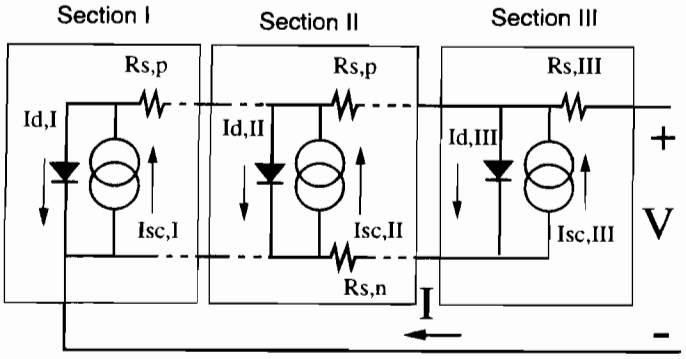


**Fig. 4.** Distributed electric equivalent circuit model for a whole back emitter unit cell with partial oxide surface passivation. External voltage is applied between n and p contacts.

### III.2. Circuit model parameters

One-dimensional calculations using PC-1D are carried out in order to determine the circuit parameters required to analyse the circuit sketched in Fig. 4. The magnitude of the current source associated with the segments of a particular section is determined from the product of the short circuit current density of a solar cell with a structure corresponding to that section times the segment area (60 μm × 1 cm). The dark saturation current of the diode is obtained from similar calculations but in the dark. The resistances $R_{s,n}$ and $R_{s,p}$ are estimated from a simple expression (Zekry & Al-Mazroo 1996) given by

$$R_{s,n,p} = 0.5\rho_{sheet,n,p}L$$

where L is the segment width and $\rho_{sheet,n,p}$ is the sheet resistance of the $n^+$ emitter or of the p-type base. Silicon to metal contact resistance and metal finger resistance are neglected but can be easily added to the model if necessary.

The conversion efficiency can now be calculated from the I–V characteristics of the circuit in Fig. 4, where I is the current flowing in the external circuit and V is the voltage applied to the p contact in section III to the n contact in section I. The cell conversion efficiency is obtained from the maximum power per unit area of the total unit cell assuming an incident optical power of 0.1 W/cm$^2$.

### III.3. Circuit analysis

#### *III.3.1. Analytical solution*

The analytical solution is initiated at the last segment in section I (metal contacted emitter), here referred to as the initial segment, and proceeds backward towards the first segment in section III, here referred to as the last segment. The total current and the external voltage are expressed as a function of the potential at node 1 of the initial segment. The nodes in all segments are numbered following the same order shown in Fig. 3. Assuming ideal diodes, the current and voltages of the segments in section I are related through:

$$I_{2,i} = I_{sc,i} - I_{d,i}\exp(V_{1,i}/V_t - 1) \quad (1)$$

$$V_{2,i} = V_{1,i} - R_{s,p}I_{2,i} \quad (2)$$

where i = 1, 2, ... n with n being the number of metal contacted segments, $I_{x,i}$ is the current flowing in the branch 1x in section i, $V_{x,i}$ is the voltage at node x in section i, $I_{sc,i}$, $I_{d,i}$ and $R_{s,p}$ are the circuit element parameters of segment i and are identical since they represent identical segments of section I and $V_t = kT/q$ is the thermal voltage (=25.8 mV at 300 K). The diodes are assumed to be ideal with an ideality factor $\eta = 1$ and the shunt resistance is neglected. The same procedure can be applied to circuits with non-ideal diodes and with shunt resistance without real difficulties. The voltage at node 3 and at node 4, $V_{3,i}$ and $V_{4,i}$ are kept at zero potential since the metal contact series resistance is neglected. Since node 2 of section i is identical to node 1 of section i + 1, $V_{2,n}$ and $I_{2,n}$ can be calculated if the values of $V_{1,1}$ and $I_{1,1}$ are known by applying (1) and (2) repetitively. From the symmetry of the structure we know that $I_{1,1} = O$ and $V_{1,1}$ is taken as an independent parameter to be used in the total current and external voltage expressions.

In the calculations of the currents and voltages through the segments of section II (oxide passivated emitter) and section III, the same elementary circuit representing section II in Fig. 4 will be used but with appropriate values for the corresponding circuit element parameters. Note that even $R_{s,n}$ will be included for the final segment as well but its value does not interfere in the calculations since the current flowing into it would be zero. In order to progress with the calculations, $V_{2,n}$ and $I_{2,n}$, resulting from the calculations across section I, are used as initial conditions. The currents and voltages through the segments of section II and III are related through

$$I_d = I_{d,i}[\exp(V_{1,i} - V_{3,i})/V_t - 1] \tag{3}$$

$$I_{2,i} = I_{1,i} + I_{sc,i} - I_d \tag{4}$$

$$V_{2,i} = V_{1,i} - R_{s,p,i} I_{2,i} \tag{5}$$

$$I_{3,i} = I_{4,i} + I_{sc,i} - I_d \tag{6}$$

$$V_{4,i} = V_{3,i} - R_{s,n,i} I_{4,i} \tag{7}$$

where i = n + 1, ... n + m + 1 with m the number of segments in section II, and $I_{sc,i}$, $I_{d,i}$, $R_{s,p,i}$ and $R_{s,n,i}$ are the circuit element parameters for segment i. An interative process is needed in order to solve the set of equations (3) through (7) subject to the boundary conditions imposed by: 1) the results of previous section namely $I_{2,n} = I_{1,n+1}$, $V_{2,n} = V_{1,n+1}$ and $V_{3,n+1} = 0$, and 2) the symmetry of the final segment leading to $I_{4,n+m+1} = 0$.

The convergence speed is determined by m, the number of segments in section II, since the right side boundary condition shifts to the left one segment per iteration. It is found that 5 to 10 extra iteration steps after the $m^{th}$ iteration are needed to come to a final solution. Iterations are performed until the total sum of changes in voltage at the different nodes and current in the different branches of the structure is insignificant. Such a linear convergence assures a very fast solution and no attempts were made to speed up convergence. Finally, the voltage and current at node 2 in the final segment represent the external voltage and total current.

By varying the starting voltage in the initial segment, a full I–V characteristic of the circuit can be extracted and the conversion efficiency is determined from the maximum power point.

This method has been used to investigate the influence of the emitter width and the width of the emitter metal contact on the cell performance. The efficiency is calculated as a function of the width for the emitter of two limiting cases of the emitter metal contact: a) minimum contact represented by 1/2 segment of metal and the rest of the emitter surface is passivated with oxide, and b) maximum contact where the whole emitter surface is covered with metal. The lateral current flow in the emitter and base causes forward biasing of the junction. By metallizing part of the emitter surface, the potential drop can be reduced. However, the dark saturation current increases in emitters with a fully metallized surface. Resolving such a trade-off leads to an optimum emitter width with as many oxide passivated segments as possible and only one metal contacted segment. This indicates that, up to a certain maximum emitter width, the effect of increasing the dark saturation current is much more deleterious to the cell performance than the lateral potential drop caused by the series resistance. For a back emitter cell 125 μm thick with $S_{n,\,eff} = 100$ cm/s and $L_n = 300$ μm, a maximum conversion efficiency of 16%, which is 2% (absolute) smaller than the one dimensional efficiency depicted in Fig. 2, was found to occur for a total number of 30 oxide passivated emitter segments separating the initial segment (emitter contact) from the final segment (base contact). To decrease the biasing of the junction caused by lateral current flow in the emitter, an extra emitter contact is inserted inside section II, as sketched in Fig. 5, resulting in an overall structure with three emitter contacts between every two successive base contacts. In this modified emitter contact structure, the junction bias is reduced because the voltage drop is divided over a smaller distance between electrodes. The analytical model presented here has been adapted to calculate the efficiency for a certain number of segments as a function of the position of the added contact. It is found that the optimum efficiency is reached when the extra contact is situated at 2/3 of the distance between the original emitter contact and the base contact. The calculated optimum efficiency of the modified structure is 16.1% which is 0.1% in absolute value greater than the efficiency of the structure having only one emitter contact.

### *III.3.2. HSPICE circuit simulations*

Numerical circuit simulations using the HSPICE circuit simulator have also been carried out in order to calculate the maximum power, and hence the efficiency, of

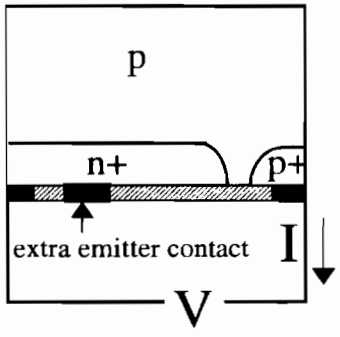


**Fig. 5.** Unit cell representing the optimum structure with a back emitter cell having a minimum back emitter contact width and an extra emitter contact segment.

the circuit in Fig. 4. The parameters of the circuit elements in the different segments have the same values used in the analytical solution detailed above. Section III is fixed and the lateral width is gradually increased by gradually increasing the number of segments in section I and section II. In a first analysis, as in the analytical calculations described above, the width of the emitter contact (section I) is fixed to its minimum possible value i.e. 1/2 segment or 30 μm, and the number of segments in section II is increased. Then the case where the whole emitter surface is metallized is treated. The resulting efficiency for both cases is plotted as a function of the total number of segments (total lateral width) in Fig. 6. For reasonably narrow emitters, the highest efficiency amounts to 16%, and occurs when the separation between the emitter contact and the base contact is 1.8 mm (30 segments), which is very close to what has been obtained analytically. For a fully metallized emitter, the maximum efficiency is 15.5% and also occurs when the separation between the emitter contact and the base contact is 1.8 mm. It appears, however, that the fully metallized emitter cell can be more advantageous than the partially metallized emitter in cells with very wide emitters (wider than 5 mm).

The front emitter unit cell sketched in Fig. 1(c) is similarly modelled using a distributed circuit and its performance simulated by means of HSPICE. The front surface metal contact width is fixed at 30 μm (half a segment width) while increasing the free surface area. Although the optical loss associated with the latter is limited to the 4% reflection loss, the conversion efficiency of the whole unit cell, however, is adjusted to take into account another 4% loss due to the bus bar coverage. As mentioned earlier, only $R_{s,n}$ associated with lateral current flow in the front emitter is considered since the back side base contact is assumed to be covering the whole back surface. A low back surface recombination velocity is, however, maintained by the effect, for example, of a back surface field diffusion. With the cell parameters described in section II.2, the peak efficiency of the front emitter surface is 17.5% as depicted in Fig. 6, which is only 0.5% (absolute) smaller than its one dimensional

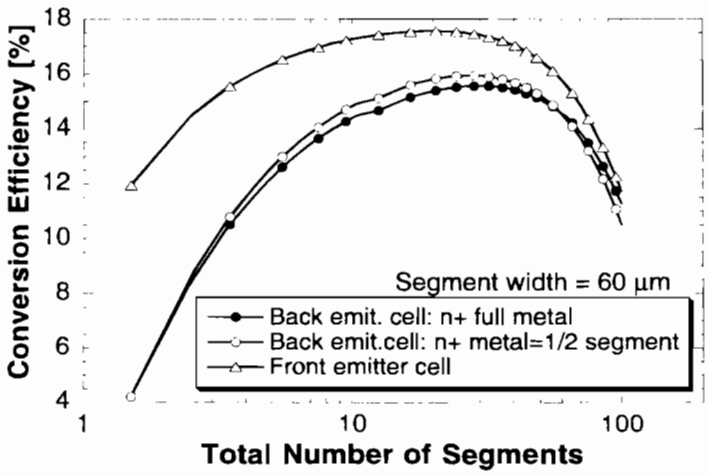


**Fig. 6.** Conversion efficiency calculated by circuit simulations with HSPICE for the distributed equivalent circuit of back emitter cells with minimum and maximum emitter contact width, and of the front emitter cell with minimum emitter contact width as a function of the lateral extension.

value seen in Fig. 2. The optimum front metal finger separation lies between 2 and 3 mm (2.4 mm) which is a reasonable spacing compared to what is encountered in practice, for instance with the screenprinting technology. It also appears from Fig. 6 that the back emitter cell performance approaches that of the front emitter cell if the separation between two adjacent metal fingers exceeds 7 mm. The efficiency in that case, however, lies well behind what can be regularly achieved with standard front emitter cell technologies and hence does not present any particular interest.

## IV. CONCLUSIONS

Using analytical and numerical calculations, it is shown here that reasonable performance of the back emitter cell fabricated on industrial material following a cost effective process is achievable at one-sun operation provided that the cell is relatively thin (thinner than 180 μm), the material is relatively good ($L_n$ longer than 300 μm) and the front surface passivation is excellent. The back emitter structure is a serious contender in thin film cells where the thickness is less than 50 μm.

The optimum back emitter cell configuration would include a reasonably well surface passivated emitter and a minimum size metal contact, or three split emitter contacts. The optimum separation between the n and p metal contact is as large as 1.5–1.8 mm, which does not present any technological difficulty.

The results obtained here show that the efficiency of dual back contact cells with a standard thickness is 1.5% absolute value lower than that of standard front emitter cells. Nevertheless, taking into account that the trend in cost effective processes is towards thinner cells, and considering the advantages of dual back contact cells in increasing the module packing density, in offering a higher degree of automation to the module assembly process with a higher yield, and hence leading to a higher production rate, the dual back contact cell can certainly be considered a serious candidate for future industrial silicon solar cells.

## ACKNOWLEDGEMENT

This work was supported by Kuwait University Research grant EE-079.

## REFERENCES

**Basore, P.A. & Clugston, D. A. 1996.** PC-1D Version 4. Proceedings of the 25th IEEE Photovoltaic Specialists Conference. Washington-DC, USA, 377–380.

**Chiang, S.Y., Carbajal, B.G. & Wakefield, G.F. 1978.** Improved Performance Thin Solar Cells. IEEE Transactions on Electron Devices **25:** 1405–1409.

**Eades, W.D. & Swanson, R.M. 1985.** Calculation of the surface generation and recombination velocities at the Si–$SiO_2$ interface. Journal of Applied Physics **58:** 4267–4276.

**Gee, J.M., Schubert, W.K. & Basore, P.A. 1993.** Emitter Wrap-Through solar cell. Proceedings of the 23rd IEEE Photovoltaic Specialists Conference. Louisville-Kentucky, USA, 265–270.

**Gee, J.M., Buck, M.E., Schubert, W.K. & Basore, P.A. 1994.** Progress on the Emitter Wrap-Through silicon solar cell. Proceedings of the 12th European Photovoltaic Solar Energy Conference. Amsterdam-The Netherlands, 743–746.

**Ghannam, M., Sivoththaman, S., Poortmans, J., Szlufcik, J., Nijs, J., Mertens, R. & Van Overstraten, R. 1997.** Trends in industrial silicon solar cell processes. Solar Energy. **59:** 101–110.

**Ghannam, M.Y. 1991.** A New $N^+PN^+$ Structure with Back Side Floating Junction for High Efficiency Silicon Solar Cell. Proceedings of the 22nd Photovoltaic Specialists Conference. Las Vegas-Nevada, USA, 284–289.

**Lammert, M.D. & Schwartz, R.J. 1977.** The Interdigitated Back Contact Solar Cell: A silicon Solar Cell for Use in Concentrated Sunlight. IEEE Transactions on Electron Devices. **24:** 337–342.

**Schwartz, R.J. 1982.** Review of silicon solar cells for high concentrations. Solar Cells **6:** 17–38.

**Sinton, R., Kwark, Y., Swirhun, S. & Swanson, R.M. 1985.** Silicon Point Contact Concentrator Solar Cells. IEEE Electron Device Letters **6:** 405–407.

**Sinton, R.A. & Swanson, R.M. 1987.** Design Criteria for Si Point-Contact Concentrator Solar Cells. IEEE Transactions on Electron Devices **34:** 2116–2123.

**Szlufcik, J., Elgamel, H.E., Ghannam, M., Nijs, J. & Mertens, R. 1991.** Simple integral screenprinting process for selective emitter polycrystalline silicon solar cells. Applied Physics Letters. **59:** 1583–1584.

**Von Roos, O. & Anspaugh, B. 1978.** The Front Surface Field Solar Cell, A New Concept. Proceedings of the 13th IEEE Photovoltaic Specialists Conference. 1119–1120.

**Zekry, A. & Al-Mazroo, A. 1996.** Distributed SPICE-Model of a Solar Cell. IEEE Transactions on Electron Devices. **43:** 691–700.

(*Accepted 24 January 1998*)

# نموذج لدارة كهربائية موزعة لتمثيل الخلايا الشمسية السيليكونية ذات الوصلة الخلفية

مصطفى غنام 1 – إيمانويل فان كرسهافر 2 و يوهان نيس 2
1- قسم الهندسة الكهربائية والكمبيوتر – جامعة الكويت ، ص.ب. 5969 – الصفاة 13060
2- الكويت مركز بحوث الإلكترونيات IMEC – جامعة لوفان – بلجيكا

## خلاصة

يعرض هذا البحث مقارنة كمية بين أداء الخلايا الشمسية السيليكونية ذات الوصلة الخلفية ونظيرتها ذات الوصلة الأمامية ، وذلك عن طريق تمثيل الخلية الشمسية بدارة كهربائية موزعة ومكونة من عدة مقاطع. يمثل كل مقطع منها خلية شمسية متناهية في الصغر. تفصل مقاومات الباعث والقاعدة بين المقطعين المتتاليين وبذلك يمكن تبسيط دراسة الخلية ، وبخاصة الخلية ذات الوصلة الخلفية بدلا من الدراسة الرقمية ذات البعدين التي تتطلب وقتا حسابيا طويلا جدا. وفي هذا النموذج يتم حساب الكميات الخاصة بمكونات الدارة باستخدام حاكي الخلايا الشمسية PC-1D. أما حساب الدارة ذاتها ، فيتم باستخدام حاكي الدارات الكهربائية HSPICE.

تظهر النتائج أن أداء الخلية الشمسية ذات الوصلة الخلفية يمكن أن يتفوق على أداء الخلية الشمسية ذات الوصلة الأمامية عندما يكون سمك الخلية رقيقا جدا (أقل من 50 ميكرون) بشرط اتقان التحييد الكهربائي للسطوح الأمامية و الخلفية.